The patterns of base changes in the two regions sequenced behave as expected from surveys of other groups of vertebrates. Transitions outnumber transversions in both segments, and silent changes outnumber replacement changes in the cytochrome *b* gene. Moreover, the rate of change in the control region exceeds that in the cytochrome *b* gene. The results give no reason to suppose that the rates of mtDNA evolution are uneven or accelerated among East African cichlid fishes.

The likelihood of extreme recency for the Victorian flock is underscored by the finding that species within the Neotropical genus *Cichlasoma* differ by as much as 11% in their cytochrome *b* sequences[7] (Fig. 1*b*), whereas the Victoria flock differs by only 5% from the Malawi flock. Indeed, no diversity in the cytochrome *b* segment (legend to Table 2) was evident within the Victoria flock. An estimate of the divergence times among the flocks is based on the assumption that the mean rate of divergence in the cytochrome *b* gene is 2.5% per million years. Our molecular results date the origin of the extant Victorian flock at less than 200,000 years ago (Fig. 2). Lake Victoria's age has been estimated to be between 250,000 and 750,000 years[15], but younger ages are considered likely for the present-day fauna[3]. This date and the other estimated divergence times (Fig. 2) fit with the estimated geological ages of the three lakes (1–2 million years (Myr) for Lake Malawi and 2–4 Myr for Lake Tanganyika[16]). So it is likely that the Victoria flock arose within the lake.

Furthermore, this result weakens the hypothesis that similarly specialized species from different lakes are more closely related to each other than to morphological generalists from the same lake. These specializations probably evolved repeatedly and independently. The establishment of the monophyly of this species flock draws attention to the remarkable speed of the morphological diversification in Lake Victoria without an acceleration of molecular evolution.

Unfortunately, we are losing the opportunity to study the cichlid fauna of Lake Victoria, because much of it is going or has gone extinct as a result of the introduction of a non-endemic predatory fish.[17,18] □

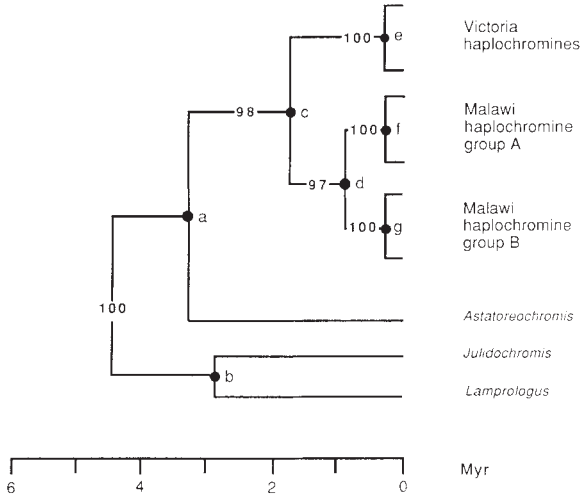

FIG. 2 Evolutionary tree for 36 African cichlid species based on a parsimony analysis[25] of mtDNA sequences. The tree is a composite based on two approaches. Only amino-acid replacement changes in cytochrome *b* were used to confirm the two deepest nodes, a and b, as well as to place the root on the ab branch, using *Hemichromis* as an outgroup. The four equally short trees obtained (each with 14 steps, consistency index CI = 0.75) did not sort out the branching order inside the group stemming from node a. A second approach used control region data with two cichlids of Lake Tanganyika (*Julidochromis* and *Lamprologus*) as the outgroup and established the branching pattern shown, with high boot-strap values (97–100)[26] confirming each of the internal branches (ab, ac, cd, ce, df and dg). The data did not allow the resolution of the relationships within any of the three assemblages stemming from nodes e, f and g (accordingly, parsimony analysis yielded nine equivalent solutions, each requiring 178 mutations; CI = 0.826). Other studies suggest that the cytochrome *b* gene diverges at a rate of at least 2.5% per million years in mammals[29]. On the basis of this rate and the per cent differences obtainable from Table 2, *Astatoreochromis* shared a common ancestor with the endemic Lake Victoria cichlids ~3.5 Myr ago, in exact agreement with the date inferred from studies of proteins encoded by nuclear genes[3]. The two main groups of cichlid fishes from Lake Malawi seem from this approach to have had a common ancestor ~700,000 years ago, the geological age of this lake being 1–2 Myr[16]. The low genetic distances observed among the proteins of the Malawi haplochromines B are consistent with this inference[27,28].

Received 30 July; accepted 20 August 1990.

1. Fryer, G. & Iles, T. D. *The Cichlid Fishes of the Great Lakes of Africa. Their Biology and Evolution* (Oliver & Boyd, Edinburgh, 1972).
2. Regan, C. T. *Proc. zool. Soc. Lond.* **1922,** 157–191 (1922).
3. Sage, R. D., Loiselle, P. V., Basasibwaki, P. & Wilson, A. C. in *Evolution of Fish Species Flocks* (eds Echelle, A. A. & Kornfield, I.) 185–201 (University of Maine Press, Orono, 1984).
4. Greenwood, P. H. *Bull. Br. Mus. nat. Hist. (Zool.)* **44,** 249–290 (1983).
5. Greenwood, P. H. *Bull. Br. Mus. nat. Hist. (Zool.)* **45,** 209–231 (1983).
6. Greenwood, P. H. *Bull. Br. Mus. nat. Hist. (Zool.)* **3,** 295–333 (1956).
7. Kocher, T. D. *et al. Proc. natn. Acad. Sci. U.S.A.* **86,** 6196–6200 (1989).
8. Vigilant, L., Pennington, R., Harpending, H., Kocher, T. D. & Wilson, A. C. *Proc. natn. Acad. Sci. U.S.A.* **86,** 9350–9354 (1989).
9. Nei, M. & Roychoudhury, A. K. *Evol. Biol.* **14,** 1–59 (1982).
10. Sage, R. D. & Selander, R. K. *Proc. natn. Acad. Sci. U.S.A.* **72,** 4669–4673 (1975).
11. Meyer, A. *Evolution* **41,** 1357–1369 (1987).
12. Avise, J. C., Bermingham, E., Kessler, L. G. & Saunders, N. C. *Evolution* **38,** 931–941 (1984).
13. Thomas, W. K. & Beckenbach, A. T. *J. molec. Evol.* **29,** 233–245 (1989).
14. Eccles, D. H. & Trewavas, E. *Malawian Cichlid Fishes. The Classification of Some Haplochromine Genera* (A. W. Diekhoff Lake Fish Movies, Herten, 1989).
15. Temple, P. H. *Biol. J. Linn. Soc.* **1,** 363–371 (1969).
16. Banister, K. E. & Clarke, M. A. *J. nat. Hist.* **14,** 483–542 (1980).
17. Barel, C. D. N. *et al Nature* **315,** 19–20 (1985).
18. Miller, D. J. *Trends Ecol. Evol.* **2,** 56–59 (1989).
19. Greenwood, P. H. *Bull. Br. Mus. nat. Hist. (Zool.)* **35,** 265–322 (1979).
20. Greenwood, P. H. *Bull. Br. Mus. nat. Hist. (Zool.)* **39,** 1–101 (1980).
21. Ribbink, A. J., Marsh, B. A., Marsh, A. C., Ribbink, A. C. & Sharp, B. J. *S. Afr. J. Zool.* **18,** 149–310 (1983).
22. Anderson, S. *et al. Nature* **290,** 457–465 (1981).
23. Gilbert, T. L. *et al. Nucleic Acids Res.* **16,** 11825 (1988).
24. Johansen, S., Guddal, P. H. & Johansen, T. *Nucleic Acids Res.* **18,** 411–419 (1990).
25. Swofford, D. L. *PAUP: Phylogenetic Analysis Using Parsimony, Version 3* (Illinois Natural History Survey, Champaign, Illinois, 1989).
26. Felsenstein, J. *Evolution* **39,** 783–791 (1985).
27. Kornfield, I. L. *Experientia* **34,** 335–336 (1978).
28. Kornfield, I. L., McKaye, K. & Kocher, T. *Isozyme Bull.* **18,** 76 1985.
29. Irwin, D. M., Kocher, T. D. & Wilson, A. C. *J. molec. Evol.* (in the press).

ACKNOWLEDGEMENTS. We thank K. Barel, R. Hoogerhoud, I. Kornfield, P. Reinthal, M. Stiassny and F. Witte for the collection and identification of specimens, I. Kornfield and P. Moran for mtDNAs of six Malawian cichlids and D. Irwin, I. Kornfield, M. Nishida, P. Reinthal and M. Stiassny, and especially E. Prager, for discussion. This work was supported by the NSF and NIH (A.C.W.), a Sloan fellowship to A.M., and an NIH fellowship to T.D.K.

Transparency and the uniqueness constraint in human and computer stereo vision

Stephen B. Pollard & John P. Frisby

AI Vision Research Unit, University of Sheffield, Sheffield S10 2TN, UK

THE sensation of depth that is obtained with human binocular vision results from the differences in the projection of the world onto the two retinae. The process entails solving the problem of stereo correspondence, which involves choosing the correct matches between left and right image features. Many computational models of stereo vision assume a uniqueness constraint on stereo matching—that is, each feature identified in one image should eventually be matched with only one feature in the other image[1,2]. This constraint would seem to be justified, as allowing non-unique matches would be tantamount to supposing that the scene entities to which matches relate are in two places at once[1]. The value of the uniqueness constraint for eliminating false matches has been demonstrated in a variety of stereo algorithms. Yet on the basis of psychophysical results Weinshall[3] concluded that it was not used by humans in dealing with certain types of ambiguous random-dot stereograms. We have now tested how Weinshall's stereograms are dealt with by PMF[4], a stereo algorithm which uses a

unique-matches selection procedure in conjunction with a purely local similar-disparity support scheme. We found that PMF produces results that are closely analogous to the psychophysical results. This suggests that Weishall's experiments should not be interpreted as evidence that the human stereo mechanism establishes non-unique matches.

With the PMF algorithm, support for each potential match is sought within a local neighbourhood from other potential matches that share similar disparities. Similarity is defined in terms of the disparity between potential matches not exceeding a moderate disparity gradient limit[5]. (Psychophysical measurements suggest that the human visual system is limited by a disparity gradient of about unity for allowable binocular fusion[6]. We exploited the disparity gradient concept to establish stereo correspondences. We view[5] the magnitude of the disparity gradient limit in PMF's local support scheme in terms of a trade-off between disambiguation power and the ability to deal with as wide a class of scene structures as possible. Gradient limits less than unity provide greater disambiguating power, and are often therefore preferable for finding matches, but at the

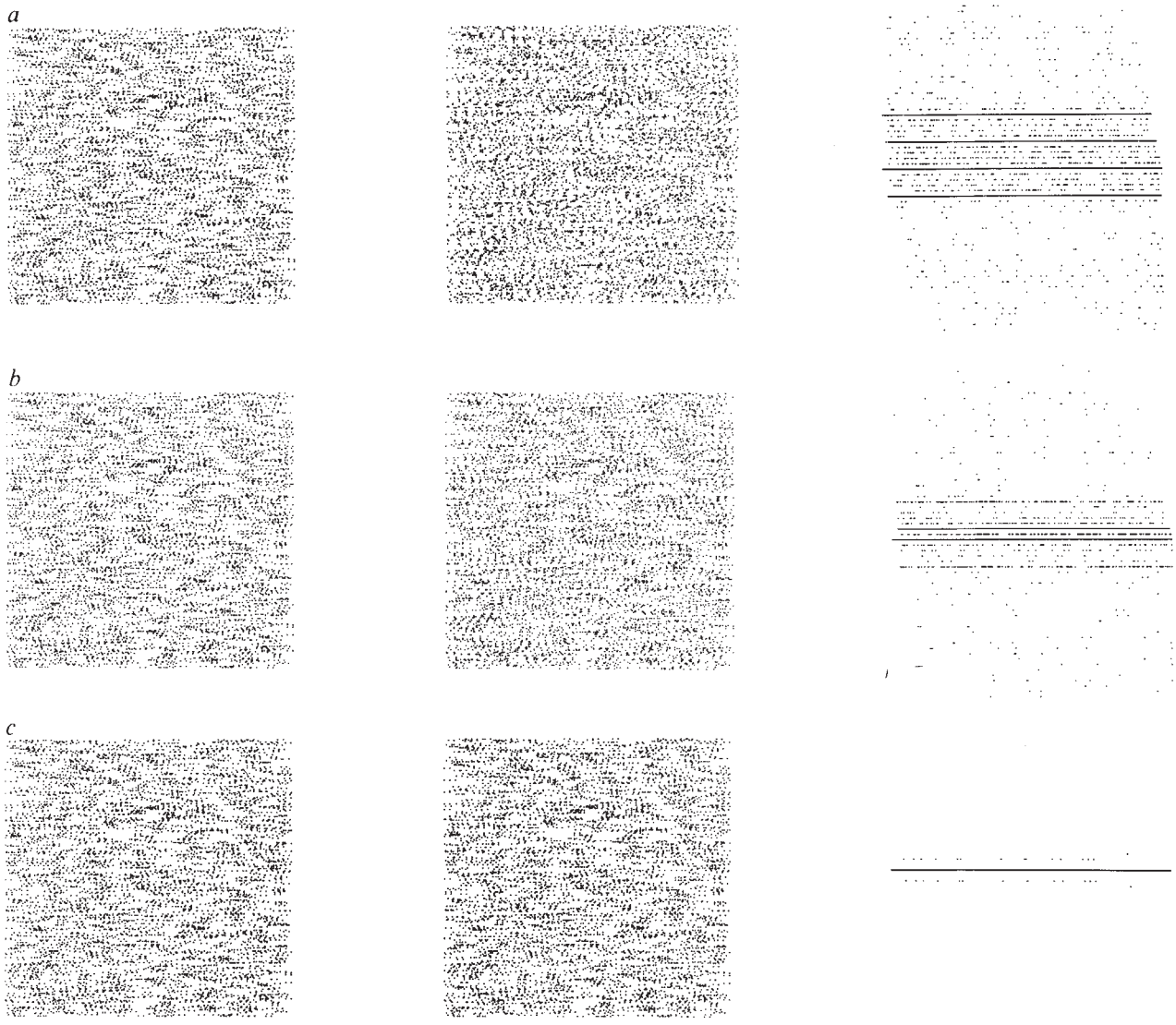

FIG. 1 Three random-dot stereograms and the results of the application of PMF to each of them. Each stereogram is constructed as follows. A 5% random dot pattern (256 units square) is replicated in the left image with a spacing between copies of G_l pixels and in the right image with spacing G_r pixels. The right-hand column shows the respective profiles through disparity space of the unique matches identified by PMF: for purposes of illustration, all matches from all over the associated stereo pair are compressed into a single cross-section, with disparity planes varying from convergent to divergent from bottom to top of the figure. For the experiments reported here, PMF's support neighbourhood was defined as a circular patch of radius 10 pixels in the left image, and the disparity range for the pool of potential matches was +/−20 pixels. In *a*, $G_l=5$ and $G_r=10$, unique matches were obtained by PMF (when run with a limiting disparity gradient of 0.5) for 5,814 of the possible 6,246 image primitives. These were distributed densely within four disparity planes so that they appear as almost solid lines in the profile figure. Psychophysical data[3] for stereograms similar to *a* are similar in that some human observers report stable fusion of up to four transparent depth planes. The inner pair of dense planes (at disparities of 0 and 5 pixels)—called the 'correct solution' in the text because they have the disparities of the two copies of the random dot texture—comprise only slightly more selected matches (1,330 and 1,226 uniquely determined matched points, respectively) than the outer pair of dense 'ghost' planes at 10 and −5 unit disparities (1,113 unique matches in each plane). This distribution reflects the marginally increased chance of matches between the correct planes exchanging support than in the ghost cases. If the disparity gradient limit used in PMF is increased to 1.0 (the psychophysical limit of fusion) qualitatively similar results are observed but the number of unique matches in the correct planes increases (1,840 and 1,716) and in the ghosts planes decreases (390 and 447). *b* ($G_l=5$ and $G_r=7$) shows that as the disparity difference between disparate copies is decreased the correct solution becomes dominant: in this case, PMF can match uniquely 5,951 matches of which most (2,351 and 2,523) exist in the inner pair of planes (at disparities of 0 and 2 pixels, respectively). *c*, Illustration of the way in which PMF selects a single surface (with 6,159 unique matches in it and a few incorrect fusions at disparities of 1 or 2 pixels from it) for the condition where $G_l=G_r=5$. This result is also in close accord with psychophysical data[3].

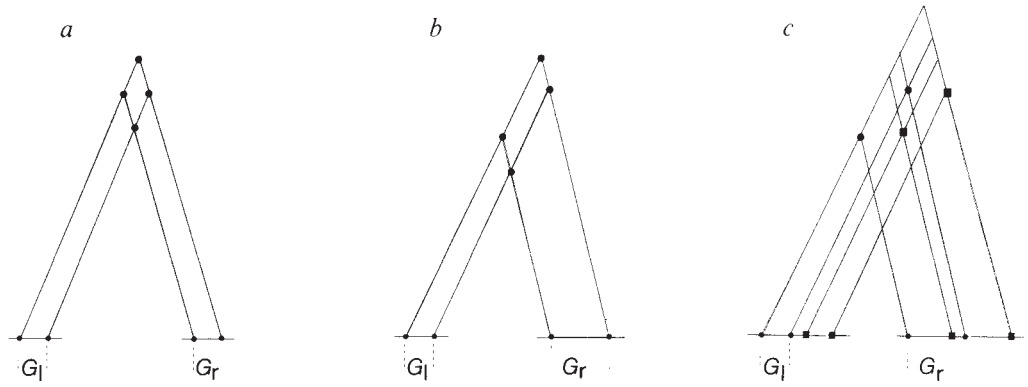

FIG. 2 Variants of the double nail illusion. *a*, Pairs of identical objects presented to humans are generally seen as lying side by side when they originate from thin objects (such as nails, needles or pins) arranged one immediately behind the other. The 'correct' solution would require a change in the order of projection of points along matching epipolar lines in the two images[7]. *b*, Asymmetric version of the same illusion. Again the order-preserving solution is preferred. *c*, Double double nail illusion. Two sets of pairs of points in the left and right images with separations G_l and G_r between copies and with $G_r = 2G_l$. If the separation in the left image between the circular and square primitives is less than G_r then a change of order in the right image results.

price of less good performance on three-dimensional surfaces varying rapidly in depth.) After calculation of support scores, matches are selected according to a winner-take-all scheme in which maximally supported matches are chosen such that only one match is permitted for each left and right image feature. This final selection stage imposes the uniqueness constraint. One important feature of the algorithm is that no cost is imposed from neighbouring matches that violate the disparity gradient limit (compare with Prazdny's similar algorithm[7]). Hence PMF can deal (to an extent dependent on particular image characteristics, see below) with partially transparent surfaces that are only locally spatially cohesive[4,7].

Figure 1 presents examples of the kind of random dot stereograms used by Weinshall and the results of applying PMF to them. The stimuli were created by first generating a random dot pattern and then constructing each stereo image by adding another copy of it, with horizontal spacing between copies in the left and right images being termed G_l and G_r respectively. Both PMF and (some) human observers interpret stereograms like Fig. 1*a*, in which $G_r = 2G_l$, as consisting of four transparent planes of dots. When $G_r = G_l$, as in Fig. 1*c*, both PMF and humans report a single plane. Computational experiments with stimuli of this kind have revealed that the number of planes appearing in the output from PMF is dependent on a complex interaction between: (1) the disparity difference between copies in the left and right images (increasing the difference strengthens the ghost planes: for example, an intermediate condition in which $G_r = 1.4G$, produces two planes, Fig. 1*b*); (2) the size of the limiting disparity gradient used in the computation of local support (increasing the limit weakens the ghost planes); and (3) density of the stereogram (increasing the density strengthens the ghost planes).

Weinshall[3] argued that the imposition of the uniqueness constraint for Fig. 1*a* should result in matches lying in just two disparity planes, one for each copy of the random dot pattern from which the stereo halves were made (these two planes will hereafter be called the 'correct' planes). At first sight this seems a reasonable claim because arriving at four planes suggests that each copy is being matched more than once. Yet the prediction rests on the assumption that each and every match reflecting the disparate positions of the two copies should obtain more support than competing 'incorrect' matches lying in other so-called 'ghost' planes. This assumption is false for an algorithm such as PMF, which incorporates only local support. The complex patterns of interference that arise between random dots in each of the potential transparent surfaces, correct and incorrect, are such that at least some incorrect matches will obtain more local support (and hence will be uniquely selected) than their correct counterparts.

Why do fewer planes emerge as the disparity difference decreases between copies in each image? The decrease leads to an increase in the probability of support existing between the correct disparity planes relative to the probability of equivalent support existing between other combinations of disparity planes. The decrease also leads to a decrease in the interference between the local support structures for dot patterns in each plane. Together these factors cause the correct solutions to become increasingly dominant with decreasing disparity difference, with unique solutions tending to be consistent with the two correct surfaces for certain values of separation (see, for example, Fig. 1*b*). The limiting case is when the disparity difference is decreased to zero, which produces a single coherent surface (as in Fig. 1*c*).

Weinshall's stereograms are designed to be random-dot extensions of the double nail illusion[8]. The latter arises from just two elements in each stereo image (Fig. 2). The reported psychophysical results, and those obtained from the application of PMF, to the random dot versions, however, reveals important differences between the two cases. At the level of dot micropatterns, it is clear that when considered in isolation, each repeated dot couplet along matching rasters in the left and right random dot images forms an individual version of a stimulus pattern for generating the double nail illusion. But at the macro level of dense random dot patterns portraying transparent surfaces, complex interactions and ambiguities occur that cannot be accounted for by treating these stimuli as enlarged versions of the double nail case. For example, consider the situation illustrated in Fig. 2*c*, which shows how the ordering of dots along a pair of matching rasters fails to be preserved because of an interaction between just a pair of double dot couplets.

Contrary to Weinshall, we conclude that just because the kind of stereogram shown in Fig. 1*a* can produce the perception of four distinct depth planes, the human visual system does not necessarily *ipso facto* fail to impose the uniqueness constraint. Indeed, the phenomenon of four depth planes supports exactly the opposite conclusion, at any rate for dense textures, insofar as a stereo algorithm that imposes unique matches also produces four depth planes for equivalent stimuli.

It would be possible in principle to devise a stereo algorithm that imposed unique matches and also produced just two depth planes for Fig. 1*a* and *b*. Such an algorithm would need to incorporate a benefit for unique matches lying in the minimum number of globally cohesive planes. The human visual system does not produce the minimum number of planes consistent with unique matches and this suggests that it may use solely local neighbourhood support interactions of the kind intrinsic to the design of PMF. □

Received 7 June; accepted 24 July 1990.

1. Marr, D. & Poggio, T. *Science* **194**, 283–287 (1976).
2. Mayhew, J. E. W. & Frisby, J. P. *Artificial Intelligence* **17**, 349–386 (1981).

3. Weinshall, D. *Nature* **341**, 737–739 (1989).
4. Pollard, S. B., Mayhew, J. E. W. & Frisby, J. P. *Perception* **14**, 449–470 (1985).
5. Pollard, S. B., Porrill, J., Mayhew, J. E. W. & Frisby, J. P. *Proc. 3rd Int. Symp. Robotics Research* 19–26 (1985).
6. Burt, P. & Julesz, B. *Perception* **9**, 671–682 (1980).
7. Prazdny, S. *Biological Cybernetics* **52**, 93–99 (1985).
8. Krol, J. D. & van de Grind, W. A. *Perception* **9**, 651–669 (1980).

ACKNOWLEDGEMENTS. We thank J. Mayhew and J. Porill for criticisms of this manuscript.

Reformation of long axon pathways in adult rat central nervous system by human forebrain neuroblasts

Klas Wictorin, Patrik Brundin, Björn Gustavii*, Olle Lindvall† & Anders Björklund

Department of Medical Cell Research, University of Lund, Biskopsgatan 5, S-22362 Lund, Sweden
* Department of Obstetrics and Gynecology, University Hospital, S-22185 Lund, Sweden
† Department of Neurology, University Hospital, S-22185 Lund, Sweden

THE failure of lesioned axons to regenerate over long distances in the mammalian central nervous system (CNS) is not due to an inability of central neurons to regenerate, but rather to the non-permissive nature of the CNS tissue environment[1–4]. Regenerating CNS axons, which grow well within a peripheral nerve, for example, fail to penetrate mature CNS tissue by more than about 1 mm[1,5,6]. Recent evidence indicates that this may be due to inhibitory membrane proteins associated with CNS oligodendrocytes and myelin[2–4,7,8]. We report here that human telencephalic neuroblasts implanted into the excitotoxically lesioned striatum of adult rats can escape or neutralize this inhibitory influence of the adult CNS environment and extend axons along major myelinated fibre tracts for distances of up to ~20 mm. The axons were seen to elongate along the paths of the striato-nigral and cortico-spinal tracts to reach the substantia nigra, the pontine nuclei and the cervical spinal cord, which are the normal targets for the striatal and cortical projection neurons likely to be present in these implants.

Rats subjected to a unilateral ibotenic acid lesion of the caudate-putamen were injected into the same area after 7–10 days or one year later with a cell suspension prepared from the telencephalic ganglionic eminences ($n = 16$) or from the rhombencephalic lip ($n = 4$) dissected from the brains of 8–10 week-old aborted fetuses (Fig. 1). The rats were immunosuppressed to prevent rejection of the xenogeneic tissue[9]. Brains were processed for immunohistochemical analysis 12–25 weeks after implantation (Fig. 1). The human neurons and their associated axonal outgrowth were visualized using a species-specific antibody raised against a constituent of human neurofilaments (HNF) that has a molecular weight of 70,000 (refs 10, 11). Control sections from intact or ibotenic acid-lesioned rat brains were completely unstained by this antibody. This was also the case for sections from transplanted brains, identical to the ones used here but carrying implants of fetal rat or mouse ganglionic eminence tissue.

Fourteen of the 20 grafted rats (12 telencephalic and 2 rhombencephalic grafts) contained viable HNF-positive implants. Nissl-stain revealed patches of mature-looking graft neurons interspersed with areas of small, immature-looking cells. The HNF-immunoreactivity was primarily confined to densely stained fibres within the well developed areas of the implants. Adjacent sections stained with antibody against the dopamine D1 receptor-related phosphoprotein DARPP-32, used as a marker for striatal projection neurons[12], revealed DARPP-32-positive and DARPP-32-negative patches within the neuron-rich areas of the telencephalic implants. This indicates that, like grafts of rat ganglionic eminence tissue[13,14], the present human telencephalic implants were composed of a mixture of striatal and non-striatal (probably, at least in part, cortical) tissue.

In seven of the brains with surviving telencephalic implants, extensive outgrowth of HNF-positive fibres occurred within the host brain (Fig. 1). The fibres could be traced in large numbers, both along the internal capsule and the cerebral peduncle caudally towards the brain stem, and along the corpus callosum and the deep layers of the cerebral cortex into large areas of the overlying cortex. The predominant fibre outgrowth was along the myelinated fibre tracts and at higher magnification (Fig. 2*a* and *b*), the HNF-positive fibres could be seen to run both within and on the surface of the individual host myelinated fibre fascicles. This long-distance fibre outgrowth also occurred in the two animals in which the striatal lesion had been made one year before the fetal cell implantation. By contrast, very little fibre outgrowth was observed from the rhombencephalic tissue implants, despite the fact that they were themselves rich in HNF-positive fibres.

The caudally directed fibres extended in slender fascicles across the caudal and medial aspects of the implant–host border, through the adjacent host striatal neuropil to join the caudally running fibre bundles of the host internal capsule (Fig. 2*d*). The HNF-positive fibres coursed caudally into and through the globus pallidus, where some of them branched or turned into this nucleus (Fig. 1*a*, and levels II and III in Fig. 1*b*). A few fibres deviated into the thalamus. Interesting branching patterns were seen, such as the one depicted in Fig. 2*c*, where the principal axon gave off a collateral branch that passed through the bundle of white matter to ramify among the cell bodies within the globus pallidus. The fibres continued as a well defined bundle in the medial part of the internal capsule, in a position similar to that of the striato-nigral and cortico-spinal pathways; along the way, axons also branched off into the subthalmic nucleus (Fig. 2*e*). In the region of the substantia nigra, some axons turned dorsolaterally into the overlying pars reticulata; others continued in the medial part of the cerebral peduncle (levels V–VI in Fig. 1*b*; and Fig. 2*f*) and could be traced in high numbers into the pontine nuclei at a distance of 8–10 mm from the implant. Some fibres were also identified in deep parts of the tectum. In the cerebral peduncle, the HNF-positive fibre bundles occupied a position similar to that of cortico-fugal axons labelled anterogradely from the fronto-parietal cortex in intact animals[15,16]. In two of the animals, where the lower brain stem and upper spinal cord were included in the analysis, HNF-positive fibres were observed in the medulla oblongata at the level of the pyramidal crossing, and in the white and grey matter of the upper cervical spinal cord at a distance ~20 mm from the implant.

The retrograde fluorescent tracers Fluoro-Gold and rhodamine-labelled latex beads were injected into the globus pallidus and substantia nigra, respectively, in two rats with telencephalic implants (Fig. 1). Clusters of Fluoro-gold-positive cell bodies and scattered cells labelled with rhodamine-latex beads were identified within the mature-looking regions of the implants, thus confirming that neurons in the implants projected to these sites.

The fibres projecting into the cortex extended in large numbers along the corpus callosum, the external capsule and the forceps minor, and within the deep layers of the cortex bilaterally. Labelled fibres were distributed in the frontal, parietal and occipital cortices on both sides. Ventrally, HNF-positive fibres could be traced into the amygdaloid-piriform area at about 8–10 mm away from the implants.

In line with the idea that the formation of long fibre tracts in the CNS reflects an interaction and balance between growth-promoting and growth-inhibiting factors along the growth trajectory, it has been proposed[2,4,7] that the limited regrowth of axotomized neurons in the adult brain or spinal cord is, at least in part, due to an active inhibition of axonal elongation exerted